AMERICAN SOCIETY FOR MICROBIOLOGY | mBio®

RESEARCH ARTICLE
Therapeutics and Prevention

Phage Resistance in Multidrug-Resistant *Klebsiella pneumoniae* ST258 Evolves via Diverse Mutations That Culminate in Impaired Adsorption

Shayla Hesse,[a] Manoj Rajaure,[a] Erin Wall,[a] Joy Johnson,[a] Valery Bliskovsky,[b]† Susan Gottesman,[a] Sankar Adhya[a]

[a]Laboratory of Molecular Biology, Center for Cancer Research, National Cancer Institute, Bethesda, Maryland, USA
[b]Laboratory of Cancer Biology and Genetics, Center for Cancer Research, National Cancer Institute, Bethesda, Maryland, USA

ABSTRACT The evolution of phage resistance poses an inevitable threat to the efficacy of phage therapy. The strategic selection of phage combinations that impose high genetic barriers to resistance and/or high compensatory fitness costs may mitigate this threat. However, for such a strategy to be effective, the evolution of phage resistance must be sufficiently constrained to be consistent. In this study, we isolated lytic phages capable of infecting a modified *Klebsiella pneumoniae* clinical isolate and characterized a total of 57 phage-resistant mutants that evolved from their prolonged coculture *in vitro*. Single- and double-phage-resistant mutants were isolated from independently evolved replicate cocultures grown in broth or on plates. Among resistant isolates evolved against the same phage under the same conditions, mutations conferring resistance occurred in different genes, yet in each case, the putative functions of these genes clustered around the synthesis or assembly of specific cell surface structures. All resistant mutants demonstrated impaired phage adsorption, providing a strong indication that these cell surface structures functioned as phage receptors. Combinations of phages targeting different host receptors reduced the incidence of resistance, while, conversely, one three-phage cocktail containing two phages targeting the same receptor increased the incidence of resistance (relative to its two-phage, nonredundant receptor-targeting counterpart). Together, these data suggest that laboratory characterization of phage-resistant mutants is a useful tool to help optimize therapeutic phage selection and cocktail design.

IMPORTANCE The therapeutic use of bacteriophage (phage) is garnering renewed interest in the setting of difficult-to-treat infections. Phage resistance is one major limitation of phage therapy; therefore, developing effective strategies to avert or lessen its impact is critical. Characterization of *in vitro* phage resistance may be an important first step in evaluating the relative likelihood with which phage-resistant populations emerge, the most likely phenotypes of resistant mutants, and the effect of certain phage cocktail combinations in increasing or decreasing the genetic barrier to resistance. If this information confers predictive power *in vivo*, then routine studies of phage-resistant mutants and their *in vitro* evolution should be a valuable means for improving the safety and efficacy of phage therapy in humans.

KEYWORDS bacteriophage cocktails, bacteriophage resistance, bacteriophage therapy

Rising rates of antibiotic resistance and the inability of drug development to keep pace has reinvigorated interest in alternative therapies, such as lytic bacteriophage (phage). The potential to harness phage lysis to control infection in humans is an old, albeit incompletely, tested concept (1, 2). Despite accumulating case reports that

Citation Hesse S, Rajaure M, Wall E, Johnson J, Bliskovsky V, Gottesman S, Adhya S. 2020. Phage resistance in multidrug-resistant *Klebsiella pneumoniae* ST258 evolves via diverse mutations that culminate in impaired adsorption. mBio 11:e02530-19. https://doi.org/10.1128/mBio.02530-19.

Editor Graham F. Hatfull, University of Pittsburgh

Address correspondence to Shayla Hesse, shayla.hesse@nih.gov, or Sankar Adhya, sa4p@nih.gov.

† Deceased.

Received 22 September 2019
Accepted 10 December 2019
Published 28 January 2020

support the therapeutic utility of phage, key questions pertaining to the broader efficacy of phage therapy remain unanswered (3–5). Selection for phage-resistant bacteria is one concern, as resistance to single phages has been shown to emerge readily *in vitro* (6, 7). How clinically significant phage resistance will be *in vivo* is a more complicated question, as host immunology, concomitant antibiotic therapy, infective bacterial inoculum, and tissue-specific physiology all are expected to play a role (8, 9).

Presumably, clinically significant phage resistance will continue to arise despite our best efforts at prevention. Even in the "successful" phage therapy case of Tom Patterson, an *Acinetobacter baumannii* isolate cultured from the patient 8 days after phage therapy initiation demonstrated resistance to all 8 phages in the initial cocktails (3). With that in mind, laboratory characterization of the most likely resistant mutants to emerge after phage-specific selection pressure is applied could constitute an important pretreatment safety measure. Phage-resistant isolates generated *in vitro* could conceivably be screened for changes in bacterial fitness, such as growth rates in various tissues and antibiotic susceptibility, which may, in turn, help avert the use of phages that select for more virulent bacterial subpopulations and help identify antibiotics that synergize with phage.

The utility of such an approach depends on two factors: (i) how consistently phage resistance evolves *in vitro* and (ii) how closely phage resistance generated *in vitro* correlates with resistance generated *in vivo*. In this paper, we addressed the former by characterizing how consistently phage resistance evolved from a clonal bacterial population exposed to lytic phages, singly or in combination, in independent replicate cocultures. The time to detectable emergence of resistance, the frequency of specific resistance-conferring mutations, and the specific step of the phage infection cycle blocked by individual mutations were compared between replicates.

Phage resistance was evolved in a derivative of the multidrug-resistant *K. pneumoniae* clinical isolate, KPNIH1, following exposure to natural phages isolated from wastewater. KPNIH1 belongs to the epidemiologically significant sequence type 258 (ST258), which has been associated with high rates of carbapenem resistance and a propensity for nosocomial transmission in countries around the world (10, 11). KPNIH1 lacks obvious CRISPR sequences and represents a unique capsular type, although its capsular polysaccharide closely resembles that of *K. pneumoniae* serotypes K19 and K34 (12). A modified derivative of KPNIH1, MKP103, was generated by Colin Manoil and colleagues through targeted knockout of the carbapenemase gene bla_{KPC-3}. MKP103 was substituted for the clinical isolate in this study in the interest of laboratory safety (13).

RESULTS

Phage isolation. Two phages that formed clear plaques on MKP103 were isolated from sewage and named Pharr (for brevity, referred to here as P1) and ϕKpNIH-2 (P2). These phages were characterized by electron microscopy, one-step growth experiments, and genome sequencing. Sequence analysis confirmed that P1 and P2 were related to strictly lytic phages and that neither phage harbored an identifiable integrase, toxin, or bacterial virulence factor, satisfying several recommended criteria for therapeutic phage selection (14).

Therapeutic phages are commonly administered as a cocktail (referring to a defined combination of phages) in an attempt to avert, or at least minimize, problems engendered by phage resistance. In order to test three-phage cocktails for their ability to suppress phage-resistant growth in MKP103, wastewater was screened for additional phages. A third phage that efficiently lysed MKP103 and proved genetically distinct from P1 and P2 was not recovered. However, two phages capable of lysing P1-resistant MKP103 (but not parental MKP103) were recovered readily and named ϕKpNIH-6 (P6) and ϕKpNIH-10 (P10).

Thus, an alternative strategy for assembling cocktails was employed, one that combines phages that infect the original bacterial target with phages that infect a phage-resistant derivative of that target. Provided that phage resistance follows con-

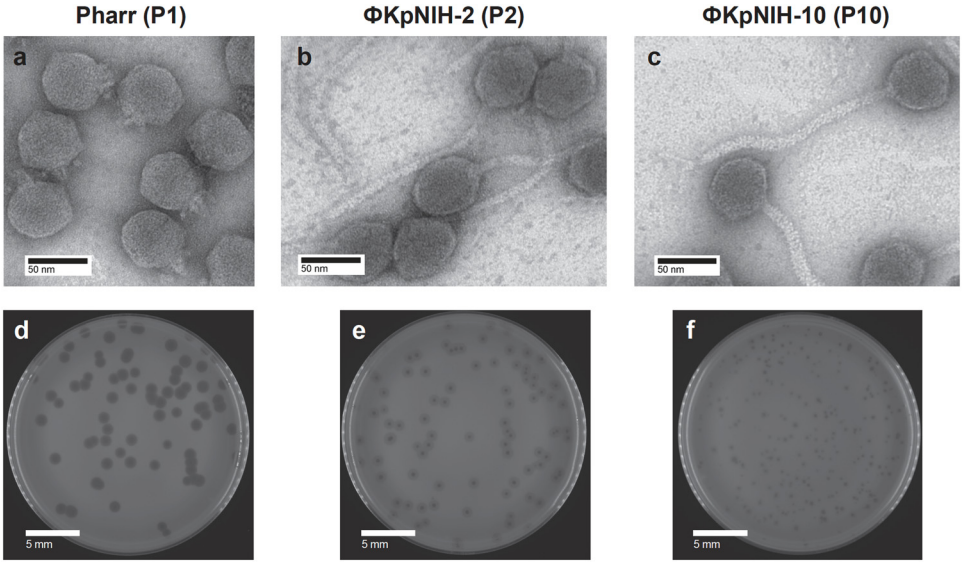

FIG 1 Structural characterization and plaque morphology of environmentally isolated phages. (a to f) Transmission electron micrographs (a to c) and plaque appearance (d to f) of Pharr, ϕKpNIH-2, and ϕKpNIH-10. The plated bacterial hosts were MKP103 (d and e) and P1+P2-resistant MKP103 (f).

sistent evolutionary pathways, one might expect this strategy to better suppress resistance to the overall cocktail. However, there is insufficient evidence at present to ascertain whether a layered cocktail approach (as exemplified by the combination of P1, P2, and P10, designated P1+P2+P10) or nonlayered approach (in which all phages target the original bacterial isolate) is categorically preferable in this regard. Cocktails of both types have shown efficacy *in vivo* (15, 16).

Phage characterization. P1 is a 40.6-kb podophage that produces large plaques on MKP103 (Fig. 1A and D). P2 is a 49.4-kb siphophage that produces medium-sized plaques on MKP103 that are surrounded by large haloes (Fig. 1B and E). P10 is a 49.5-kb siphophage that produces small plaques on P1+P2-resistant MKP103 (Fig. 1C and F). P6, a 172-kb predicted myophage, proved unable to infect P1+P2-resistant MKP103 and was not imaged. A schematic of the host specificity for each phage appears in Fig. S1 in the supplemental material.

P1 lysis and P2 lysis of MKP103 each occurred within 20 min in microtiter plates (Fig. 2A). P10 lysis of P1+P2-resistant MKP103 took twice the time to reach a plateau (~40 min), which may just reflect the lower growth rate of its host (Fig. 2B and Table S1). The onset of P1 lysis preceded that of P2 and also proceeded at a higher rate, which correlated with a shorter latent period and smaller burst size for P1 versus P2 infection. A summary comparison of these two phages, along with P6 and P10, is shown in Table 1. P6 plaque morphology and lysis of its host, P1-resistant MKP103, in planktonic culture appear in Fig. S2.

Phage resistance evolution. P1-, P2-, and P1+P2-resistant populations grew out from bacterium-phage cocultures after prolonged incubation, while P1+P2+P10 resistance did not (Fig. 2C). Phage resistance was selected in lysogeny broth (LB) as well as on LB-agar plates to assess whether evolved resistance varied by culture method (17). Ten replicate planktonic cocultures and ten replicate phage spots for each phage group (P1, P2, and P1+P2) were compared on the basis of time to resistant mutant outgrowth as well as the overall frequency with which resistant populations emerged.

High temporal consistency was observed among independent planktonic cocultures that produced P1-resistant and P2-resistant outgrowth (Fig. 2C). P1+P2 resistance emerged over a wider range of time and, in some cases, not at all. All P1+P2-resistant populations that did grow out did so after the single-phage-resistant populations, suggesting that dual-phage resistance was not conferred by resistance to either phage

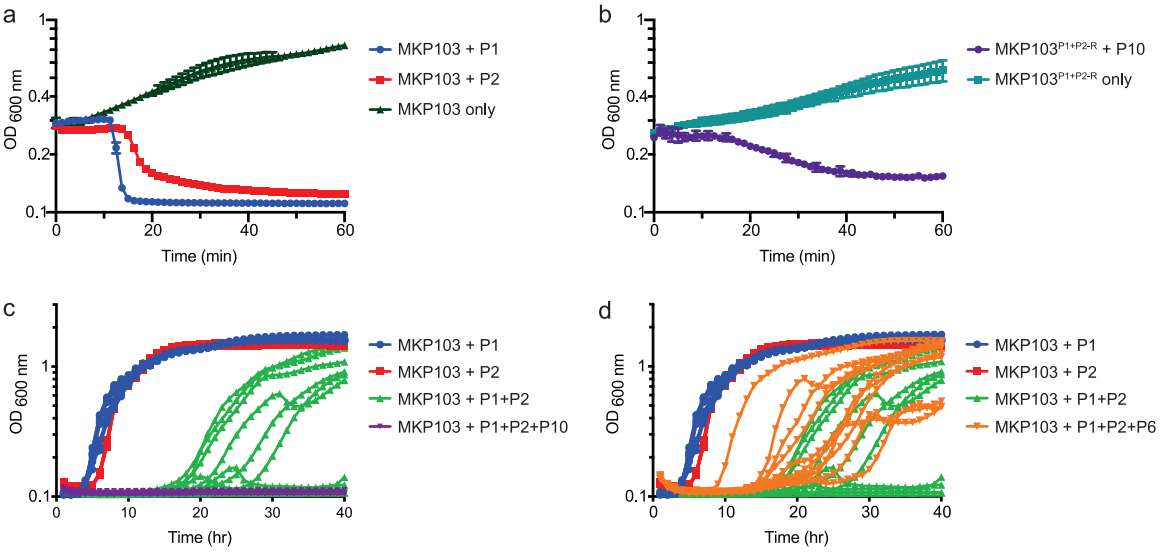

FIG 2 Phage lysis and resistant bacterial outgrowth. (a and b) Phage lysis of host bacterial cultures in a shaking incubator at a multiplicity of infection (MOI) of 3. Error bars denote standard deviations among triplicate samples. MKP103$^{P1+P2-R}$, P1+P2-resistant MKP103. (c and d) Growth of phage-resistant bacterial populations over time in cocultures of MKP103-phage. For each phage or phage combination, data from 10 independent cocultures were plotted. Total MOI remained constant (P1, MOI of 6; P2, MOI of 6; P1+P2, MOI of 3 + 3; P1+P2+P10, MOI of 2 + 2 + 2; P1+P2+P6, MOI of 2 + 2 + 2). P1, Pharr; P2, ϕKpNIH-2; P6, ϕKpNIH-6; P10, ϕKpNIH-10.

alone. Real-time coevolution between bacteria and phage, manifesting as sinusoidal oscillations in culture density, was observed in select P1+P2 replicates.

Adding a third phage to the P1+P2 combination had opposing effects. Whereas P1+P2+P10 suppressed resistant outgrowth in all 10 replicates, P1+P2+P6 led to earlier and more frequent outgrowth of resistance than P1+P2 alone (Fig. 2C and D).

On solid-state media, the order in which resistant colonies became apparent mirrored the order in which resistance in broth culture emerged: P1 and then P2, followed by P1+P2 (Fig. 3). The relative abundance of resistant colonies per phage spot decreased in like order.

Phage-resistant populations that evolved in broth were diluted and plated to isolate colonies. One colony from each planktonic culture or phage spot was subjected to three rounds of colony purification (in the absence of phage selection) before being reassessed for phage resistance. Three putative P2-resistant isolates demonstrated P2 susceptibility after colony purification; all 57 others demonstrated heritable resistance. All subsequent characterization of resistance was performed on clonal isolates generated in this manner.

Delineation of cross-resistance patterns. Each phage-resistant isolate was evaluated for resistance to P1, P2, and P10 individually. Plated isolates were classified as resistant, partially resistant, and susceptible based on the appearance of overlying

TABLE 1 Summary phage comparison[a]

Parameter	Pharr (P1)	ϕKpNIH-2 (P2)	ϕKpNIH-6 (P6)	ϕKpNIH-10 (P10)
Structural classification	*Podoviridae*	*Siphoviridae*		*Siphoviridae*
Selected host	MKP103	MKP103	P1-resistant MKP103	P1+P2-resistant MKP103
Plaque morphology				
Lytic center	+++	++	+	+
Halo	−	+++	−	−
Canonical phage type	T7-like	T1-like	T4-like	T1-like
Genome size (bp)	40,599	49,477	171,860	49,472
Growth kinetics				
Latent period, min [means (SD)]	16 (1)	24 (1)	22 (1)	22 (1)
Burst size, PFU [means (SD)]	18 (1)	57 (24)	45 (15)	26 (2)

[a]+, ++, and +++, relative size of attribute; −, attribute not visibly appreciable.

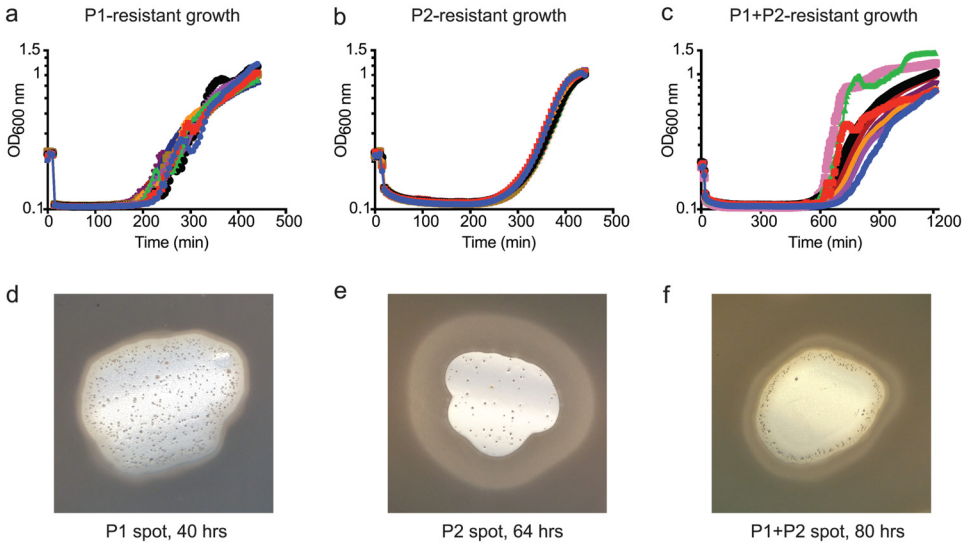

FIG 3 P1-, P2-, and P1+P2-resistant mutant generation in planktonic culture and on plates. (a to c) Outgrowth of planktonic bacterial populations with resistance to P1, P2, and P1+P2, respectively. Each panel depicts growth from 10 independent MKP103-phage coculture replicates, from which one colony-purified isolate from each was sequenced. Replicates in panel c were selected from a pool in order to exclude replicates in which phage resistance was not detectable by an increase in optical density. (d to f) Appearance of colonies with resistance to P1, P2, and P1+P2. Photos of phage spots were taken at 40 h (d), 64 h (e), and 80 h (f) after phage plating.

phage spots (Fig. S3A). All P1-resistant isolates were fully susceptible to P2 and vice versa (Fig. S3B and C). All P1-resistant isolates were P10 susceptible, all P2-resistant isolates were P10 resistant, and most (18/20) P1+P2-resistant isolates were partially or fully susceptible to P10 (Fig. S3D). The two completely P10-resistant isolates retained partial susceptibility to P1 and P2, suggesting that complete resistance to all three phages is either rare or lethal in MKP103.

Quantitation of phage adsorption. Bacterial mutation causing phage receptor loss, alteration, or masking is one of the most common mechanisms of phage resistance (7). In such a mutant, phage can no longer be adsorbed, and measurement of free (unadsorbed) phage following a brief incubation period can reveal defects in attachment and binding that are required for phage infection. By this assay method, adsorption was impaired for all P1-, P2-, and P1+P2-resistant isolates following incubation with the specific phage or phages to which they had evolved resistance (Fig. 4). Adsorption at a set time point (see Materials and Methods) was ~100-fold less for most phage-resistant isolates relative to that of the parental MKP103 strain. The exceptions included all P2-resistant isolates and two P1+P2-resistant isolates (planktonic 5 and 8), for which adsorption was only ~10-fold less than that of parental MKP103. A likely explanation for the less severe adsorption impairment observed among P2-resistant isolates became apparent after genome sequencing.

Identification of resistance mutations. To identify mutations responsible for conferring phage resistance, genomic DNA from each bacterial isolate was extracted, sequenced, and mapped to the KPNIH1 reference genome (GenBank accession no. NZ_CP008827). High-probability mutations (defined as high-frequency, non-silent mutations within an open reading frame) were selected for further vetting.

The KPNIH1 transposon mutant library generated by Colin Manoil's laboratory at the University of Washington was used to selectively test for phage resistance resulting from the loss of function of a single gene (13). Twenty-three mutants with a transposon insertion in one of fifteen genes found to harbor a high-probability mutation by sequencing analysis (some genes with >1 transposon insertion) were obtained and tested for phage resistance via spot test. Eight genes had a corresponding transposon mutant that demonstrated resistance to the expected phage(s). Only one gene containing a high-probability mutation did not have a corresponding transposon mutant

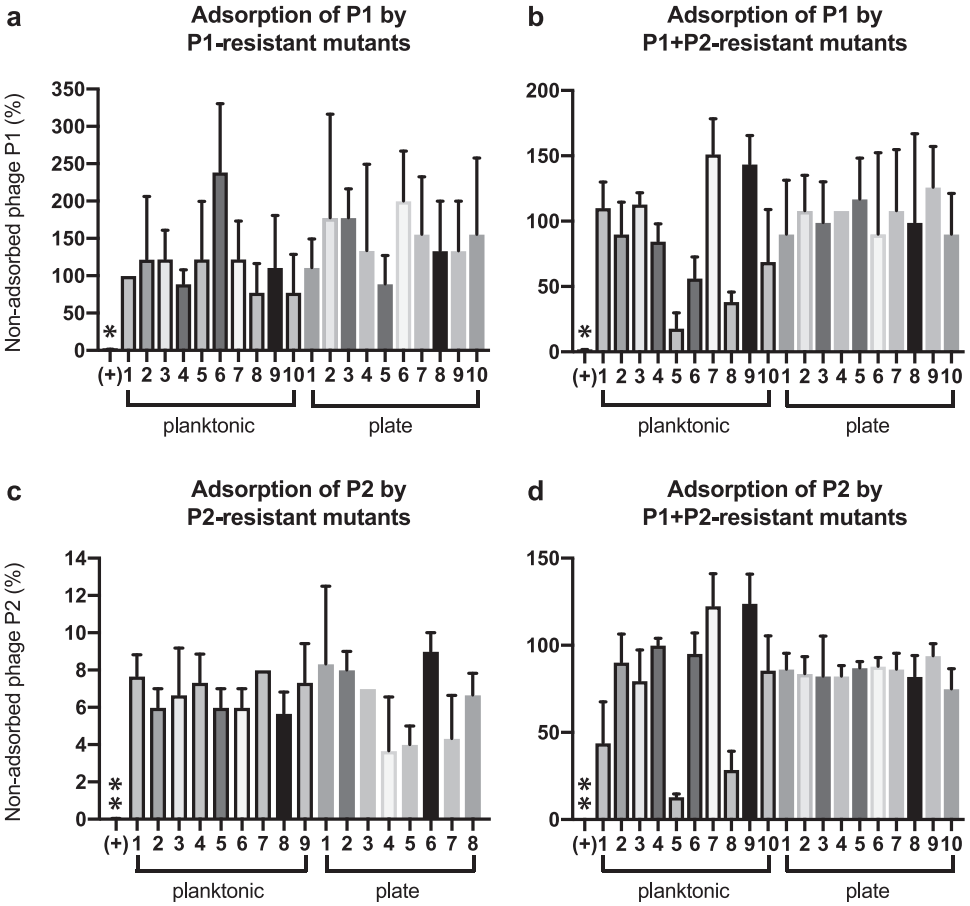

FIG 4 Phage adsorption among resistant isolates. Free phage titers were measured after brief incubation with each phage-resistant bacterial isolate and calculated as a percentage of phage recovered from the medium-only condition. (a and b) Adsorption of phage P1 by P1-resistant and P1+P2-resistant isolates. (c and d) Adsorption of phage P2 by P2-resistant and P1+P2-resistant isolates. Error bars denote standard deviations among triplicate samples. Free phage recovery following incubation with MKP103, denoted by (+), was minimal. *, 1.2% (P1); **, 0.04% (P2).

(*wbaP*). A summary of mutations detected in these 9 genes (8 confirmed by comparison to transposon mutants plus *wbaP*) is shown in Table 2. Seven high-probability mutations failed experimental confirmation (based on their corresponding transposon mutants being phage-susceptible) and are listed in Table S2.

The tests with transposon mutants demonstrated that inactivation of specific genes is sufficient to produce resistance. To confirm that the identified mutations are necessary for resistance in the more complex phenotype of the evolved strains, plasmid-based complementation tests were performed. Complementation was judged to have occurred if the vector-insert transformant regained significant phage susceptibility without the requirement of fully recapitulating parental MKP103 susceptibility (Fig. S4).

All resistance mutations confirmed by a specific transposon mutant also could be complemented, with the exception of 4 large deletion mutants (for which complementation with a single plasmid construct was not attempted) and 2 single-nucleotide variant (SNV) mutations in *wzc* (P1-resistant planktonic 7 and plate 1 mutants). Wzc, an integral inner membrane protein that forms part of a transenvelope capsule translocation complex, also facilitates polymerization of capsular polysaccharide when activated by its tyrosine autokinase domain, making it conceivable that point mutations in *wzc* could be dominant to the wild type (18, 19). Notably, two frameshift *wzc* mutants in the group could be complemented.

For a number of isolates, no candidate resistance mutation was identified and/or confirmed. This may have been due to intergenic mutations affecting gene regulation,

TABLE 2 Summary of identified phage resistance mutations and tests of complementation[a]

Resistant isolate	Mutation[b]	Putative gene function	Complementation	
			Yes	No
P1-R planktonic 1	*Rham* Y220fs	Rhamnosyltransferase	*Rham*	*wzc*
P1-R planktonic 2	None confirmed		*wzc*	
P1-R planktonic 3	None confirmed		*wzc*	
P1-R planktonic 4	None confirmed		*wzc*	
P1-R planktonic 5	None confirmed		*wzc*	
P1-R planktonic 6	None confirmed		*wzc*	
P1-R planktonic 7	*wzc* A354T	Capsule synthesis		*wzc*
P1-R planktonic 8	*wbaP* L387R	Cell envelope biogenesis	*wbaP*	*wzc*
P1-R planktonic 9	None confirmed		*wzc*	
P1-R planktonic 10	None confirmed		*wzc*	
P1-R plate 1	*wzc* R292P	Capsule synthesis		*wzc*
P1-R plate 2	None confirmed		*wzc*	
P1-R plate 3	None confirmed		*wzc*	
P1-R plate 4	None confirmed		*wzc*	
P1-R plate 5	None confirmed		*wzc*	
P1-R plate 6	*Rham* N270fs	Rhamnosyltransferase	*Rham*	*wzc*
P1-R plate 7	*wzc* K345fs	Capsule synthesis	*wzc*	
P1-R plate 8	*wzc* E24fs	Capsule synthesis	*wzc*	
P1-R plate 9	None confirmed		*wzc*	
P1-R plate 10	None confirmed		*wzc*	
P2-R planktonic 1	*ompC* Y301ps	Outer membrane porin	*ompC*	
P2-R planktonic 2	*wabH* N92V	LPS synthesis	*wabH*	
P2-R planktonic 3	*wabH* P225f	LPS synthesis	*wabH*	
P2-R planktonic 4	*wabH* N92V	LPS synthesis	*wabH*	
P2-R planktonic 5	*wabH* N92V	LPS synthesis	*wabH*	
P2-R planktonic 6	*wabH* N92V	LPS synthesis	*wabH*	
P2-R planktonic 7	None confirmed		*ompC*	*wabH*
P2-R planktonic 8	*wabH* N92V	LPS synthesis	*wabH*	
P2-R planktonic 9	None confirmed		*ompC*	*wabH*
P2-R plate 1	*waaF* Y287N	LPS synthesis	*waaF*	
P2-R plate 2	*ompC* N332fs	Outer membrane porin	*ompC*	
P2-R plate 3	*wabH* I191fs	LPS synthesis	*wabH*	
P2-R plate 4	*waaQ* W308ps	LPS synthesis	*waaQ*	
P2-R plate 5	*waaC* L264Q	LPS synthesis	*waaC*	
P2-R plate 6	*ompC* N332fs	Outer membrane porin	*ompC*	
P2-R plate 7	*waaQ* P163fs	LPS synthesis	*waaQ*	
P2-R plate 8	*wabH* I191fs	LPS synthesis	*wabH*	
P1+P2-R planktonic 1	None confirmed		*galU*	
P1+P2-R planktonic 2	Large deletion	Includes *cps* locus		*galU*
P1+P2-R planktonic 3	Large deletion	Includes *cps* locus		*galU*
P1+P2-R planktonic 4	None confirmed		*galU*	
P1+P2-R planktonic 5	None confirmed		*galU*	
P1+P2-R planktonic 6	None confirmed		*galU*	
P1+P2-R planktonic 7	Large deletion	Includes *cps* locus		*galU*
P1+P2-R planktonic 8	None confirmed		*galU*	
P1+P2-R planktonic 9	None confirmed		*galU*	
P1+P2-R planktonic 10	*galU* N47K	Carbohydrate metabolism	*galU*	
P1+P2-R plate 1	*galU* V12G	Carbohydrate metabolism	*galU*	
P1+P2-R plate 2	None confirmed		*galU*	
P1+P2-R plate 3	None confirmed		*galU*	
P1+P2-R plate 4	None confirmed		*galU*	
P1+P2-R plate 5	*galU* V12G	Carbohydrate metabolism	*galU*	
P1+P2-R plate 6	Large deletion	Includes *cps* locus		*galU*
P1+P2-R plate 7	None confirmed		*galU*	
P1+P2-R plate 8	None confirmed		*galU*	
P1+P2-R plate 9	None confirmed		*galU*	
P1+P2-R plate 10	None confirmed		*galU*	

[a]Chromosomal mutations in phage-resistant isolates were assessed for their likelihood to confer phage resistance based on sequencing criteria and recapitulation of the resistant phenotype by a corresponding gene transposon mutant. Mutations satisfying these criteria appear in the table, along with the results of single-gene complementation testing.

[b]*Rham*, rhamnosyltransferase; fs, frameshift; ps, premature stop.

mutations in multiple genes that collectively led to resistance, gain-of-function mutations, or epigenetic modification. Isolates without a confirmed resistance mutation were experimentally transformed with plasmid constructs that had been generated to complement other resistant mutants. Interestingly, all of these isolates could be complemented, demonstrating that provision of the particular wild-type gene product was at least sufficient to abrogate resistance (Table 2).

P1 resistance via loss of capsule. P1-resistant isolates were found to harbor mutations in three genes: a putative rhamnosyltransferase gene, *wbaP,* and *wzc*. As mentioned earlier, *wzc* plays an integral role in capsular polysaccharide surface assembly for type 1 capsule *Escherichia coli* and *Klebsiella pneumoniae* strains (18). Reference strains of *K. pneumoniae* that lack *wzc* (and its cognate phosphatase *wzb*) are acapsular (20).

In *Salmonella enterica*, WbaP is a membrane enzyme that initiates O-antigen synthesis by catalyzing the transfer of galactose-1-phosphate (Gal-1-P) onto the carrier lipid undecaprenyl phosphate (Und-P) (21, 22). However, in *K. pneumoniae* and *E. coli* K-12, proteins with high sequence similarity to WbaP have been shown to be involved in capsule synthesis (23–25).

The putative rhamnosyltransferase did not display high sequence similarity to any formally named gene or gene product, although it is suggestive that its gene, along with *wzc*, flanks *wbaP* in KPNIH1's chromosome and therefore is in close proximity to (if not included within) KPNIH1's capsule biosynthesis (*cps*) locus.

P2 resistance via truncated LPS or mutated *ompC*. Mutations conferring P2 resistance were identified in 5 genes: *waaC*, *waaF*, *waaQ*, *wabH*, and *ompC*. The *waa* gene cluster (homologous to *rfa* in *E. coli*) encompasses genes that synthesize and modify the hexose region of the lipopolysaccharide (LPS) core in stepwise fashion (26, 27). WaaC is involved in the addition of HepI to KdoI of the inner core and WaaF in the addition of HepII to HepI, and WaaQ appears to be involved in the addition of HepIII to the outer core (28, 29). All three are presumed heptosyltransferases, and null mutations in cognate gene *rfaC* or *rfaF* yield deep, rough mutants in *E. coli* and *S.* Typhimurium (27, 30). The gene *wabH*, an *rfaG* homologue, constitutes part of the same locus. WabH catalyzes the transfer of GlcNAc from UDP-GlcNAc to the outer core, and *wabH* mutants also produce truncated LPS (29, 31).

The presence of the outer membrane porin OmpC in this otherwise exclusive group of glycosyltransferases involved in core LPS synthesis may seem curious at first, but it has clear precedent. The classic *E. coli* phage T4 binds OmpC from *E. coli* K-12 and LPS from *E. coli* B, enabling it to infect both strains. Even more improbably, T4 binding to OmpC and LPS has been shown to be mediated by the same protein, long tail fiber protein 37 (32, 33).

In the case of P2, loss or alteration of either OmpC or LPS in MKP103 was sufficient to confer P2 resistance, implying that both structures are necessary for efficient phage infection. Whether P2 tail fibers interact with both, either sequentially or simultaneously, during the process of adsorption was not investigated, but adsorption codependence on two cell surface structures has been documented for multiple phages (34–36).

P1+P2 resistance via *galU* deficiency or a large deletion. Since dual-phage resistance required roughly twice as much time as single-phage resistance to reach the same threshold of detection, it was speculated that P1+P2 resistance may be mediated through sequential acquisition of P1 and P2 resistance mutations. Instead, P1+P2 resistance was associated with single-gene mutations in *galU* or large (>20-kb) chromosomal deletions that did not contain *galU*. UTP:α-D-glucose-1-phosphate uridylytransferase, the enzyme encoded by *galU*, plays a central role in cell envelope synthesis, galactose metabolism, and trehalose metabolism (37–39). More specifically, this enzyme catalyzes the synthesis of UDP-glucose, which serves as a building block for LPS, capsular polysaccharide, and osmoregulated periplasmic glucans (OPGs). Despite significantly slower bacterial growth associated with mutations in *galU* (Table S1), it

may have been the only gene for which loss of function is both nonlethal and capable of conferring P1 and P2 resistance.

Four large-deletion mutants were identified, each with slightly different deletion boundaries encompassing ~29 to 50 kb (Fig. S5). All deletions overlapped the *cps* locus and therefore included the putative rhamnosyltransferase, *wbaP*, and *wzc* genes implicated in P1 resistance. The loss of which additional gene or combination of genes led to P2 resistance is unclear. None of the genes implicated in P2 resistance were contained within any deletion, and no deletion contained prominent genes involved in LPS transport to the outer membrane (e.g., *msbA*, *lptA-G*) (40). The UDP-glucose dehydrogenase gene *ugd* as well as several epimerase genes were located in the region of overlap for all 4 deletions and were deemed the most likely candidates to account for P2 resistance in these mutants.

Sequentially evolved P1+P2 resistance. Since P1+P2 resistance did not evolve via additive gene mutations from single-phage-resistant mutants (e.g., *wzc* plus *wabH*), we wondered whether this was due to the genetic improbability of a double mutant or its lethality. To address this question, P1+P2 resistance was set up to evolve sequentially. Ten independent cultures of P1-resistant planktonic mutant 7 (with identified *wzc* mutation) were exposed to phage P2 under the same conditions used to evolve all planktonic mutants in this study. Resistance to P2 evolved readily on this P1-resistant background, emerging after a length of time very similar to that seen for P2 resistance on the MKP103 background (Fig. S6).

Two isolates from sequentially evolved P1+P2-resistant populations were submitted for sequencing of *wabH*, the gene most frequently mutated in P2-resistant mutants. Both isolates were found to harbor the same F294fs (frameshift) mutation in *wabH* and both regained P2 susceptibility with complementation, suggesting that genetic improbability, not lethality, accounts for the lack of additive resistance mutations seen in coincidentally evolved P1+P2-resistant populations.

Analysis of three-phage cocktail resistance. The addition of P6 or P10 to P1+P2 had divergent effects on the timing and frequency with which resistance to these three-phage cocktails emerged (Fig. 2C and D). To better understand the basis for this difference, P6-resistant and P10-resistant populations were evolved on a P1-resistant background, and a clonal isolate from each population was sequenced. The P1+P6-resistant mutant contained a Q88fs (frameshift) mutation in *waaZ*, a gene shown to be involved in the transfer of KdoIII to KdoII in *E. coli* K-12 core oligosaccharide (41). The P1+P10-resistant mutant contained a Q568ps (premature stop) mutation in *fhuA*, the gene encoding the ferrichrome-iron receptor of *E. coli* (42). Both mutants could be resensitized to P6 or P10 by transformation with wild-type (MKP103-derived) *waaZ* or *fhuA*, respectively, suggesting that the inability of P6 and P10 to infect parental MKP103 stems from an inability to access their receptors in the presence of capsule. Consistent with this, neither P6 nor P10 produces plaques with visible halos, unlike P2, whose plaques are surrounded by large halos. A plaque-associated halo implies the activity of phage-derived polysaccharide depolymerase, and it is this activity that likely enables P2 to bind its outer membrane receptors on MKP103 (43).

The fact that *waaZ* forms part of the *waa* gene cluster, which was heavily represented among P2 resistance mutations, suggests that P6, like P2, recognizes host LPS. On the other hand, FhuA, the putative phage receptor of P10, comprises a distinct cell surface structure not associated with resistance to either P1 or P2 (i.e., capsular polysaccharide, LPS, and OmpC). Coupling these determinations with the suppression of resistance mediated by P1+P2+P10 and the vulnerability to resistance displayed by P1+P2+P6 suggests that phage receptor diversity predicts the relative barrier to resistance imposed by a particular cocktail combination better than sheer phage quantity.

DISCUSSION

In this study, we characterized two lytic phages, Pharr (P1) and ϕKpNIH-2 (P2), as well as single- and double-phage resistance patterns in their host, MKP103. For all 57

phage-resistant mutants isolated (20 P1 resistant, 17 P2 resistant, and 20 P1+P2 resistant), we observed impaired phage adsorption. Consistent with this result, we identified resistance mutations in genes whose products are involved in the synthesis/assembly of cell surface structures or serve as cell surface structures themselves. P1 resistance mutations clustered around capsule synthesis, P2 around LPS synthesis or OmpC structure/function, and P1+P2 around carbohydrate metabolism catalyzed by GalU. Therefore, bacterial receptors of P1 and P2 were inferred to be capsular polysaccharide and LPS with or without OmpC, respectively.

The primary aim of this study was to characterize how consistently and by what pathways phage resistance in MKP103 evolves *in vitro*. In doing so, we hoped to gain an indication of how well phage resistance might be predicted based on the genetic and phenotypic characterization of a few resistant isolates. Our data suggest that although independently evolved phage-resistant MKP103 mutants can be expected to harbor different mutations conferring phage resistance, their phenotypes are likely to be similar or identical to each other. Other groups who have characterized appreciable numbers of phage-resistant mutants of *E. coli* and *Listeria monocytogenes* have arrived at similar conclusions, supporting the generalizability of this finding (44, 45).

These results may interest those seeking assurance that phages selected for therapeutic use do not, in turn, select for hypervirulent bacterial strains. Relatively few phage-resistant mutants may need to be screened in order to predict what the majority of phage-resistant mutants will look like. However, it should be emphasized that the success of such an approach could be limited by (i) different evolutionary trajectories under *in vitro* versus *in vivo* conditions, (ii) disparate physiologic effects of phenotypically similar mutants (e.g., LPS mutants with unique defects in core oligosaccharide triggering different degrees of immune activation), and (iii) greater variability in evolved bacterial resistance mechanisms (e.g., in strains containing CRISPR-Cas).

Secondary conclusions from this study include the observations that evolved phage resistance patterns were not materially affected by bacterial cultivation in broth versus bacterial cultivation on plates. However, there were markedly different resistance patterns and time to resistant outgrowth between coincidentally evolved and sequentially evolved P1+P2-resistant mutants, suggesting the presence of a significant inoculum effect. Finally, and perhaps most importantly, laboratory characterization of phage-resistant mutants, besides serving as a screen for genotypes/phenotypes associated with hypervirulence and antibiotic resensitization, may also facilitate intelligent cocktail design. Combining phages that target unique host receptors may increase the frequency of cocktails akin to P1+P2+P10, which durably suppressed resistance despite conditions highly conducive to bacterial growth. Prioritizing phage receptor diversity in the design of therapeutic cocktails may also help avoid counterproductive combinations, like the addition of P6 to P1+P2, although the extent to which P6's adverse effect on resistance is attributable to phage receptor overlap between P2 and P6 is unclear at present.

Consistent trends in MKP103's phage resistance evolution have been highlighted, but its stochastic aspects merit consideration as well. Phage-resistant mutants from replicate cocultures exhibited a range of resistant phenotypes (some grew equally well in the presence/absence of phage, while others displayed various degrees of growth inhibition) as well as a range of adsorption deficiencies, neither of which was fully accounted for by our genetic analysis. Although this degree of phenotypic variability may not be clinically significant *per se*, it is significant that it evolved under highly uniform laboratory conditions. The phenotypic range of phage-resistant mutants evolved *in vivo*, even in controlled animal models, may be much wider (46). Further characterization of phage resistance evolution, both *in vitro* and *in vivo*, is needed to determine if/how data like those presented here can be used to guide therapeutic phage selection going forward.

MATERIALS AND METHODS

Phage isolation. Pharr was isolated by Jason Gill and colleagues at Texas A&M and ϕKpNIH-2, ϕKpNIH-6, and ϕKpNIH-10 by the authors. Untreated wastewater was screened for MKP103-specific

phages according to previously described methods (15). Briefly, powdered LB medium was mixed with raw sewage (3%, wt/vol). MKP103 culture was added to LB-sewage (1:100, vol/vol) and incubated overnight. The following day the mixture was centrifuged and the supernatant passed through a 0.45-μm filter. The filtrate was mixed with MKP103 in molten soft agar and plated. Plaques were subjected to three rounds of plaque purification according to standard procedures (47).

Phage purification. Phage lysates were extracted with 1:10 (vol/vol) chloroform and centrifuged at 6,500 $\times$ *g* for 10 min. Collected supernatant was passed through a 0.45-μm filter and centrifuged at 12,000 $\times$ *g* for 10 h at 4°C. Phage pellets were resuspended in gelatin-free SM buffer (10 mM $MgSO_4$, 50 mM Tris-HCl, pH 7.5, 100 mM NaCl) and applied to a cesium chloride density gradient as described in protocols of the Jonathan King laboratory (48). The extracted phage band was transferred to a Thermo Scientific Slide-A-Lyzer dialysis cassette (10,000 molecular weight cutoff) and dialyzed against high-salt SM buffer (1 M NaCl) for 12 h and then against SM buffer (100 mM NaCl) two times for 4 h each time.

Transmission electron microscopy. Cesium gradient-purified phage preparations were applied to glow-discharged Formvar-carbon 400 mesh copper grids. Samples were washed and negatively stained with 2% uranyl acetate. Images were acquired with a JEM 1200EX transmission electron microscope (JEOL USA, Peabody, MA) equipped with an AMT XR-60 digital camera (Advanced Microscopy Techniques Corporation, Woburn, MA) at an accelerating voltage of 80 kV.

Phage adsorption and one-step growth parameters. Latent period and burst size were measured according to protocols of the Jeffrey Barrick laboratory (49–51). Phage adsorption was measured indirectly for each resistant bacterial isolate by quantifying free phage in solution following brief bacterial coculture at a multiplicity of infection (MOI) of 0.01. Briefly, bacterial isolates were grown in LB medium to an optical density at 600 nm (OD_{600}) of 0.35, and then 2 ml was transferred to 3 separate wells of a 12-well tissue culture plate. Filtered phage lysate (5×10^6 PFU in 10 μl) was added to each well, and the plate was incubated at 37°C with shaking at 140 rpm. For P1, a 10-min incubation period was followed by centrifugation at 10,000 $\times$ *g* for 5 min. For P2, an 8-min incubation was followed by extraction with 1:4 (vol/vol) chloroform and then centrifugation at 5,000 $\times$ *g* for 1 min. Lower centrifugal force was applied to P2 to avoid pelleting. For both P1 and P2, the supernatant was serially diluted and nonadsorbed phage was quantified by spot titer.

Bacterial growth rates. Growth rates of selected phage-resistant mutants were determined using the protocol for microtiter plate readers described by Barry G. Hall and colleagues (52). Briefly, frozen bacterial stocks were thawed and used to inoculate cultures grown overnight under oxygen-limited conditions and containing rich medium. The following day, inocula from overnight cultures were added to individual wells of a 96-well microtiter plate. LB broth was added to each well to constitute a 200-μl total culture volume with starting OD_{600} between 0.05 and 0.1. Plates were incubated at 37°C in a microplate reader with shaking at 150 rpm. OD readings were acquired every 5 min. Absorbance data were analyzed with GrowthRates software package, version 3.0.

Screen for phage cross-resistance. Bacterial isolates were plated using the soft-agar overlay technique. Phages P1, P2, and P10 were applied to the solidified top agar in 5-μl spots of 10^3, 10^4, and 10^9 PFU/ml. Plates were incubated overnight and assessed for phage susceptibility the following day.

Generation of phage lysis curves and phage-resistant bacterial outgrowth. Bacterial lysis and growth curves were constructed from sequential OD readings acquired on a microplate reader. Lysis curves were generated following addition of cesium-purified phage (MOI of 3) to a growing bacterial culture at an OD_{600} of 0.25. Cultures were incubated at 37°C and shaken at 180 rpm with OD readings taken every 60 s. Phage-resistant planktonic populations were generated via coculture of cesium-purified phage(s) (aggregate MOI of 6) and a growing MKP103 culture at an OD_{600} of 0.25. Cultures were incubated at 37°C and shaken at 150 rpm with OD readings taken every 5 min. Phage-resistant colonies were generated on Terrific broth (TB) plates with a soft agar-MKP103 top layer. High-titer phage (10^9 PFU/ml) was plated in 10-μl spots. Plates were incubated until visible colonies grew within the areas of clear phage lysis.

Phage genome sequencing and analysis. Genomic DNA was extracted from high-titer, cesium-purified phage preparations with phenol-chloroform and SDS according to The Actinobacteriophage Database protocol (53). Phage genomes were sequenced on Illumina MiSeq (300-bp paired reads) and assembled/annotated using the CPT Galaxy platform (54).

Bacterial genome sequencing and analysis. Bacterial genomic DNA was extracted with commercial kits (Wizard genomic DNA purification kit [Promega] and DNeasy blood and tissue kit [Qiagen]) and sequenced on the Illumina NextSeq platform (150-bp paired reads). Reads were assembled by mapping to the KPNIH1 reference genome (GenBank accession no. NZ_CP008827). Variant analysis was performed using CLC Genomics Workbench 11 (Qiagen).

Cloning. PCR to generate linearized pBAD33 vector and gene fragments with 15-bp homology ends was performed with CloneAmp HiFi PCR premix (TaKaRa Bio) under the recommended thermocycling conditions. Genomic DNA from parental MKP103 was used as the template for the latter. Cloning strategies and primer design were developed with the aid of Geneious software (version 9.1.8). Primer sequences appear in Table S3 in the supplemental material. PCR products were purified with the QIAquick PCR purification kit (Qiagen). Circularized plasmids containing the wild-type gene insert were assembled with an In-Fusion HD cloning kit (TaKaRa Bio) and used to transform competent *E. coli* cells via heat shock. Transformants were selected by growth on 175 μg/ml chloramphenicol plates. Individual colonies were picked and expanded in culture, and their plasmid DNA was extracted with a QIAprep Spin Miniprep kit (Qiagen). Faithful replication of the gene inserts as well as proper ligation into the pBAD33 vector were confirmed by Sanger sequencing.

Complementation. Phage-resistant isolates were rendered electrocompetent according to the Bio-Rad MicroPulser electroporation apparatus operating instructions and applications guide, section 5 (165-2100). After repetitive washes, a 50-μl cell suspension was mixed with 1 μg plasmid DNA and loaded into a 1-mm electroporation cuvette. Cells were subjected to a single 1.8-kV pulse shock in a Bio-Rad MicroPulser system and then immediately transferred to prewarmed SOC medium and incubated for 1 h before plating on LB agar with 175 μg/ml chloramphenicol. Expression of the wild-type gene insert was induced by exposure to 2% arabinose, followed by incubation for 1 to 12 h before phage challenge. To control for the metabolic effects of arabinose, bacterial isolates transformed with empty vector and exposed to arabinose were tested in parallel.

Data availability. Annotated phage genomes were deposited in GenBank and assigned the following accession numbers: MK618658 (P1), MN395286 (P2), MN395284 (P6), and MN395285 (P10).

SUPPLEMENTAL MATERIAL

Supplemental material is available online only.

FIG S1, EPS file, 2.7 MB.

FIG S2, EPS file, 2.4 MB.

FIG S3, EPS file, 2.9 MB.

FIG S4, EPS file, 2.4 MB.

FIG S5, EPS file, 1.9 MB.

FIG S6, EPS file, 2.4 MB.

TABLE S1, DOCX file, 0.01 MB.

TABLE S2, DOCX file, 0.01 MB.

TABLE S3, DOCX file, 0.01 MB.

ACKNOWLEDGMENTS

We gratefully acknowledge Bill Brower (DC Water) in addition to Mark Miller and colleagues (NIH Division of Environmental Protection) for help with wastewater collection. Transmission electron microscopy images were obtained with assistance from Erin Stempinski at the Electron Microscopy Core of the National Heart, Lung, and Blood Institute (NHLBI). Next-generation sequencing was performed with assistance from Valery Bliskovsky at the CCR Genomics Core of the National Cancer Institute. The Center for Phage Technology (CPT) Galaxy team at Texas A&M University, including Cory Maughmer and Mei Liu, generously provided assistance with phage genome annotation.

This work was supported by the Intramural Research Program of the National Institutes of Health, National Cancer Institute, Center for Cancer Research.

S.H., M.R., E.W., J.J., V.B., S.G., and S.A. contributed to study conception and design. S.H. and J.J. performed experiments. S.G. and S.A. supervised the study. S.H. wrote the manuscript. All authors approved the manuscript, excepting V.B. (deceased).

REFERENCES

1. Salmond GP, Fineran PC. 2015. A century of the phage: past, present and future. Nat Rev Microbiol 13:777–786. https://doi.org/10.1038/nrmicro3564.
2. Hesse S, Adhya S. 2019. Phage therapy in the twenty-first century: facing the decline of the antibiotic era; is it finally time for the age of the phage? Annu Rev Microbiol 73:155–174. https://doi.org/10.1146/annurev-micro-090817-062535.
3. Schooley RT, Biswas B, Gill JJ, Hernandez-Morales A, Lancaster J, Lessor L, Barr JJ, Reed SL, Rohwer F, Benler S, Segall AM, Taplitz R, Smith DM, Kerr K, Kumaraswamy M, Nizet V, Lin L, McCauley MD, Strathdee SA, Benson CA, Pope RK, Leroux BM, Picel AC, Mateczun AJ, Cilwa KE, Regeimbal JM, Estrella LA, Wolfe DM, Henry MS, Quinones J, Salka S, Bishop-Lilly KA, Young R, Hamilton T. 2017. Development and use of personalized bacteriophage-based therapeutic cocktails to treat a patient with a disseminated resistant Acinetobacter baumannii infection. Antimicrob Agents Chemother 61:e00954-17. https://doi.org/10.1128/AAC.00954-17.
4. Chan BK, Turner PE, Kim S, Mojibian HR, Elefteriades JA, Narayan D. 2018. Phage treatment of an aortic graft infected with Pseudomonas aeruginosa. Evol Med Public Health 2018:60–66. https://doi.org/10.1093/emph/eoy005.
5. Dedrick RM, Guerrero-Bustamante CA, Garlena RA, Russell DA, Ford K, Harris K, Gilmour KC, Soothill J, Jacobs-Sera D, Schooley RT, Hatfull GF, Spencer H. 2019. Engineered bacteriophages for treatment of a patient with a disseminated drug-resistant Mycobacterium abscessus. Nat Med 25:730–733. https://doi.org/10.1038/s41591-019-0437-z.
6. Hancock RE, Reeves P. 1975. Bacteriophage resistance in Escherichia coli K-12: general pattern of resistance. J Bacteriol 121:983–993.
7. Labrie SJ, Samson JE, Moineau S. 2010. Bacteriophage resistance mechanisms. Nat Rev Microbiol 8:317–327. https://doi.org/10.1038/nrmicro2315.
8. Roach DR, Leung CY, Henry M, Morello E, Singh D, Di Santo JP, Weitz JS, Debarbieux L. 2017. Synergy between the host immune system and bacteriophage is essential for successful phage therapy against an acute respiratory pathogen. Cell Host Microbe 22:38–47. https://doi.org/10.1016/j.chom.2017.06.018.
9. Segall AM, Roach DR, Strathdee SA. 2019. Stronger together? Perspectives on phage-antibiotic synergy in clinical applications of phage therapy. Curr Opin Microbiol 51:46–50. https://doi.org/10.1016/j.mib.2019.03.005.
10. Snitkin ES, NISC Comparative Sequencing Program Group, Zelazny AM, Thomas PJ, Stock F, Group N, Henderson DK, Palmore TN, Segre JA. 2012. Tracking a hospital outbreak of carbapenem-resistant Klebsiella pneu-

moniae with whole-genome sequencing. Sci Transl Med 4:148ra116. https://doi.org/10.1126/scitranslmed.3004129.
11. Pitout JD, Nordmann P, Poirel L. 2015. Carbapenemase-producing Klebsiella pneumoniae, a key pathogen set for global nosocomial dominance. Antimicrob Agents Chemother 59:5873–5884. https://doi.org/10.1128/AAC.01019-15.
12. Kubler-Kielb J, Vinogradov E, Ng WI, Maczynska B, Junka A, Bartoszewicz M, Zelazny A, Bennett J, Schneerson R. 2013. The capsular polysaccharide and lipopolysaccharide structures of two carbapenem resistant Klebsiella pneumoniae outbreak isolates. Carbohydr Res 369:6–9. https://doi.org/10.1016/j.carres.2012.12.018.
13. Ramage B, Erolin R, Held K, Gasper J, Weiss E, Brittnacher M, Gallagher L, Manoil C. 2017. Comprehensive arrayed transposon mutant library of Klebsiella pneumoniae outbreak strain KPNIH1. J Bacteriol 199:e00352-17. https://doi.org/10.1128/JB.00352-17.
14. Philipson CW, Voegtly LJ, Lueder MR, Long KA, Rice GK, Frey KG, Biswas B, Cer RZ, Hamilton T, Bishop-Lilly KA, Philipson C, Voegtly L, Lueder M, Long K, Rice G, Frey K, Biswas B, Cer R, Hamilton T, Bishop-Lilly K. 2018. Characterizing phage genomes for therapeutic applications. Viruses 10:188. https://doi.org/10.3390/v10040188.
15. Regeimbal JM, Jacobs AC, Corey BW, Henry MS, Thompson MG, Pavlicek RL, Quinones J, Hannah RM, Ghebremedhin M, Crane NJ, Zurawski DV, Teneza-Mora NC, Biswas B, Hall ER. 2016. Personalized therapeutic cocktail of wild environmental phages rescues mice from Acinetobacter baumannii wound infections. Antimicrob Agents Chemother 60:5806–5816. https://doi.org/10.1128/AAC.02877-15.
16. Gu J, Liu X, Li Y, Han W, Lei L, Yang Y, Zhao H, Gao Y, Song J, Lu R, Sun C, Feng X. 2012. A method for generation phage cocktail with great therapeutic potential. PLoS One 7:e31698. https://doi.org/10.1371/journal.pone.0031698.
17. Clokie MRJ, Kropinski AM. 2009. Bacteriophages: methods and protocols. Humana Press, New York, NY.
18. Whitfield C. 2006. Biosynthesis and assembly of capsular polysaccharides in Escherichia coli. Annu Rev Biochem 75:39–68. https://doi.org/10.1146/annurev.biochem.75.103004.142545.
19. Wugeditsch T, Paiment A, Hocking J, Drummelsmith J, Forrester C, Whitfield C. 2001. Phosphorylation of Wzc, a tyrosine autokinase, is essential for assembly of group 1 capsular polysaccharides in Escherichia coli. J Biol Chem 276:2361–2371. https://doi.org/10.1074/jbc.M009092200.
20. Pan YJ, Lin TL, Chen YH, Hsu CR, Hsieh PF, Wu MC, Wang JT. 2013. Capsular types of Klebsiella pneumoniae revisited by wzc sequencing. PLoS One 8:e80670. https://doi.org/10.1371/journal.pone.0080670.
21. Wang L, Liu D, Reeves PR. 1996. C-terminal half of Salmonella enterica WbaP (RfbP) is the galactosyl-1-phosphate transferase domain catalyzing the first step of O-antigen synthesis. J Bacteriol 178:2598–2604. https://doi.org/10.1128/jb.178.9.2598-2604.1996.
22. Saldias MS, Patel K, Marolda CL, Bittner M, Contreras I, Valvano MA. 2008. Distinct functional domains of the Salmonella enterica WbaP transferase that is involved in the initiation reaction for synthesis of the O antigen subunit. Microbiology 154:440–453. https://doi.org/10.1099/mic.0.2007/013136-0.
23. Arakawa Y, Wacharotayankun R, Nagatsuka T, Ito H, Kato N, Ohta M. 1995. Genomic organization of the Klebsiella pneumoniae cps region responsible for serotype K2 capsular polysaccharide synthesis in the virulent strain Chedid. J Bacteriol 177:1788–1796. https://doi.org/10.1128/jb.177.7.1788-1796.1995.
24. Drummelsmith J, Whitfield C. 1999. Gene products required for surface expression of the capsular form of the group 1 K antigen in Escherichia coli (O9a:K30). Mol Microbiol 31:1321–1332. https://doi.org/10.1046/j.1365-2958.1999.01277.x.
25. Stevenson G, Andrianopoulos K, Hobbs M, Reeves PR. 1996. Organization of the Escherichia coli K-12 gene cluster responsible for production of the extracellular polysaccharide colanic acid. J Bacteriol 178:4885–4893. https://doi.org/10.1128/jb.178.16.4885-4893.1996.
26. Regue M, Izquierdo L, Fresno S, Jimenez N, Pique N, Corsaro MM, Parrilli M, Naldi T, Merino S, Tomas JM. 2005. The incorporation of glucosamine into enterobacterial core lipopolysaccharide: two enzymatic steps are required. J Biol Chem 280:36648–36656. https://doi.org/10.1074/jbc.M506278200.
27. Schnaitman CA, Klena JD. 1993. Genetics of lipopolysaccharide biosynthesis in enteric bacteria. Microbiol Rev 57:655–682.
28. Regue M, Climent N, Abitiu N, Coderch N, Merino S, Izquierdo L, Altarriba M, Tomas JM. 2001. Genetic characterization of the Klebsiella pneumoniae waa gene cluster, involved in core lipopolysaccharide biosynthesis. J Bacteriol 183:3564–3573. https://doi.org/10.1128/JB.183.12.3564-3573.2001.
29. Aquilini E, Azevedo J, Merino S, Jimenez N, Tomas JM, Regue M. 2010. Three enzymatic steps required for the galactosamine incorporation into core lipopolysaccharide. J Biol Chem 285:39739–39749. https://doi.org/10.1074/jbc.M110.168385.
30. Wilkinson RG, Gemski P, Jr, Stocker BA. 1972. Non-smooth mutants of Salmonella typhimurium: differentiation by phage sensitivity and genetic mapping. J Gen Microbiol 70:527–554. https://doi.org/10.1099/00221287-70-3-527.
31. Frirdich E, Vinogradov E, Whitfield C. 2004. Biosynthesis of a novel 3-deoxy-D-manno-oct-2-ulosonic acid-containing outer core oligosaccharide in the lipopolysaccharide of Klebsiella pneumoniae. J Biol Chem 279:27928–27940. https://doi.org/10.1074/jbc.M402549200.
32. Yu F, Mizushima S. 1982. Roles of lipopolysaccharide and outer membrane protein OmpC of Escherichia coli K-12 in the receptor function for bacteriophage T4. J Bacteriol 151:718–722.
33. Montag D, Hashemolhosseini S, Henning U. 1990. Receptor-recognizing proteins of T-even type bacteriophages. The receptor-recognizing area of proteins 37 of phages T4 Tula and Tulb. J Mol Biol 216:327–334. https://doi.org/10.1016/S0022-2836(05)80324-9.
34. Riede I. 1987. Receptor specificity of the short tail fibres (gp12) of T-even type Escherichia coli phages. Mol Gen Genet 206:110–115. https://doi.org/10.1007/bf00326544.
35. Heller K, Braun V. 1982. Polymannose O-antigens of Escherichia coli, the binding sites for the reversible adsorption of bacteriophage T5+ via the L-shaped tail fibers. J Virol 41:222–227.
36. Baptista C, Santos MA, São-José C. 2008. Phage SPP1 reversible adsorption to Bacillus subtilis cell wall teichoic acids accelerates virus recognition of membrane receptor YueB. J Bacteriol 190:4989–4996. https://doi.org/10.1128/JB.00349-08.
37. Fukasawa T, Jokura K, Kurahashi K. 1962. A new enzymic defect of galactose metabolism in Escherichia coli K-12 mutants. Biochem Biophys Res Commun 7:121–125. https://doi.org/10.1016/0006-291x(62)90158-4.
38. Schulman H, Kennedy EP. 1977. Identification of UDP-glucose as an intermediate in the biosynthesis of the membrane-derived oligosaccharides of Escherichia coli. J Biol Chem 252:6299–6303.
39. Weissborn AC, Liu Q, Rumley MK, Kennedy EP. 1994. UTP: alpha-D-glucose-1-phosphate uridylyltransferase of Escherichia coli: isolation and DNA sequence of the galU gene and purification of the enzyme. J Bacteriol 176:2611–2618. https://doi.org/10.1128/jb.176.9.2611-2618.1994.
40. Sperandeo P, Martorana AM, Polissi A. 2017. The lipopolysaccharide transport (Lpt) machinery: a nonconventional transporter for lipopolysaccharide assembly at the outer membrane of Gram-negative bacteria. J Biol Chem 292:17981–17990. https://doi.org/10.1074/jbc.R117.802512.
41. Frirdich E, Lindner B, Holst O, Whitfield C. 2003. Overexpression of the waaZ gene leads to modification of the structure of the inner core region of Escherichia coli lipopolysaccharide, truncation of the outer core, and reduction of the amount of O polysaccharide on the cell surface. J Bacteriol 185:1659–1671. https://doi.org/10.1128/jb.185.5.1659-1671.2003.
42. Neilands JB. 1982. Microbial envelope proteins related to iron. Annu Rev Microbiol 36:285–309. https://doi.org/10.1146/annurev.mi.36.100182.001441.
43. Hughes KA, Sutherland IW, Clark J, Jones MV. 1998. Bacteriophage and associated polysaccharide depolymerases–novel tools for study of bacterial biofilms. J Appl Microbiol 85:583–590. https://doi.org/10.1046/j.1365-2672.1998.853541.x.
44. Perry EB, Barrick JE, Bohannan BJ. 2015. The molecular and genetic basis of repeatable coevolution between Escherichia coli and bacteriophage T3 in a laboratory microcosm. PLoS One 10:e0130639. https://doi.org/10.1371/journal.pone.0130639.
45. Denes T, den Bakker HC, Tokman JI, Guldimann C, Wiedmann M. 2015. Selection and characterization of phage-resistant mutant strains of Listeria monocytogenes reveal host genes linked to phage adsorption. Appl Environ Microbiol 81:4295–4305. https://doi.org/10.1128/AEM.00087-15.
46. De Sordi L, Lourenco M, Debarbieux L. 2019. I will survive: a tale of bacteriophage-bacteria coevolution in the gut. Gut Microbes 10:92–99. https://doi.org/10.1080/19490976.2018.1474322.
47. Sambrook J, Fritsch EF, Maniatis T. 1989. Molecular cloning: a laboratory manual, 2nd ed. Cold Spring Harbor Laboratory Press, Cold Spring Harbor, N.Y.

48. Haase-Pettingell C. 2000. CsCl step gradient to purify phage. http://web.mit.edu/king-lab/www/cookbook/cscl_grad_phage.htm. Accessed September 2017.
49. Heineman RH, Bull JJ. 2007. Testing optimality with experimental evolution: lysis time in a bacteriophage. Evolution 61:1695–1709. https://doi.org/10.1111/j.1558-5646.2007.00132.x.
50. Brown C. 2018. Measuring lysis timing of T7 phage. http://barricklab.org/twiki/bin/view/Lab/ProtocolsPhageLysisTiming. Accessed 12 June 2019.
51. Brown C. 2017. Measuring burst size of T7 phage. http://barricklab.org/twiki/bin/view/Lab/ProtocolsPhageBurstSize. Accessed 12 June 2019.
52. Hall BG, Acar H, Nandipati A, Barlow M. 2014. Growth rates made easy. Mol Biol Evol 31:232–238. https://doi.org/10.1093/molbev/mst187.
53. Russell DA, Hatfull GF. 2017. PhagesDB: the actinobacteriophage database. Bioinformatics 33:784–786. https://doi.org/10.1093/bioinformatics/btw711.
54. Afgan E, Baker D, Batut B, van den Beek M, Bouvier D, Cech M, Chilton J, Clements D, Coraor N, Gruning BA, Guerler A, Hillman-Jackson J, Hiltemann S, Jalili V, Rasche H, Soranzo N, Goecks J, Taylor J, Nekrutenko A, Blankenberg D. 2018. The Galaxy platform for accessible, reproducible and collaborative biomedical analyses: 2018 update. Nucleic Acids Res 46:W537–W544. https://doi.org/10.1093/nar/gky379.